University of Guilan

Computational Sciences and Engineering

Journal homepage: https://cse.guilan.ac.ir/

Thermal-Fluidic Study of Drying Chamber of Photovoltaic-powered Forced Convection Solar Dryer using Finite Element Method

M. G. Sobamowo [a,] *, A. B. Ajayi [a], O.A. Adeleye [b], M. O. Oyekeye [a]

[a] Department of Mechanical Engineering, University of Lagos, Nigeria.
[b] Department of Biomedical Engineering, University of Lagos, Nigeria.

ARTICLE INFO

Article history:
Received 20 May 2022
Received in revised form 17 June 2022
Accepted 01 July 2022
Available online 01 July 2022

Keywords:
Finite Element Simulation
Drying chamber
Heat transfer
Forced Convection
Solar dryer

ABSTRACT

Forced convection solar dryer has been widely used for effective drying of agricultural products because it permits better ventilation which makes it less dependent on weather conditions and removes moisture faster, hence preventing stagnation. Though the solar dryer has proved its usefulness, its major obstacle in its applications is the optimization of its performance. For the future sustenance of the solar dryers, the design, development, and optimization must depend on thorough theoretical tools. Hence, the current study presents the finite element analysis simulation of forced convective heat transfer in a photo voltaic-powered solar dryer. For performance optimization in the solar dryer analysis, the effects of the following factors such as blower speeds, the chamber ratio of the solar dryer, on the pressure and temperature distributions as well as the velocity in the drying chamber were investigated. From the results, the performance of the drying chamber increases as its aspect ratio decreases and as the blower speed increases. The results of this work could therefore be used in the design of an optimized Photovoltaic-ventilated forced convection solar dryer.

1. Introduction

Solar radiation is abundantly available in the tropical and subtropical regions and this has proved that solar energy can be the most desirable option for energy source in drying. The traditional method of drying agricultural products which involves open air drying is a technique in food preservation that lowers the contents of moisture in agricultural products. This process prevents the food from deterioration within the period known for safe storage. However, this technique is labour intensive,

* Corresponding author, Email mikegbeminiyiprof@yahoo.com

https://dx.doi.org/10.22124/cse.2022.22338.1031

time consuming, and large space demanding. In fact, crops get damaged and also considerable losses occur due to hostile weather conditions, human vandalism, rodents, birds, insects, rain and microorganisms. This method is proned to contamination by foreign materials and pest infestation resulting in serious degradation in the quality of food and makes the food inedible. All these lead to significant impaired quality and product loss. Consequently, quite a number of study and work have been done in the application of solar radiation knowledge which includes fabrication, production, and distribution of various solar dryers in developing countries [1-5]. However, these solar dryers are neither available in the tropics nor in the subtropics. Evaluating and optimising the performance of such systems have been the major concern and interest of most researchers of the systems. In order to achieve this, extensive studies have been done in the simulation and optimization of natural convective solar dryers for agricultural products [6-13]. The success rate of natural convection solar dryers is not encouraging because of inadequate flow of induced air. Therefore, forced convection solar drying which permits better ventilation by joining a suction fan power-driven by a solar Photovoltaic module was incorporated. This shows an improved performance as it makes the dryer less dependent on weather conditions and removes moisture faster, hence it prevents stagnation. Literatures abound on performance studies concerning forced convection solar dryers [9, 14-18]. Most of the work done as found in the literature were based on the products drying behaviour and to the best of our knowledge, little or no attention was given to the drying characteristic and performance of the drying chamber. Moreover, the finite element method is assumed to be useful for only Computational Solid Mechanics or conductive heat transfer problems in Thermo-Fluid mechanics. In fact, the Galerkin Method in the finite element methods is easily applied for heat transfer conduction problems. But when the same Galerkin Method is applied to solve convection problems, the obtained results will be substantially marred with false oscillations in space if critical values of certain parameters are exceeded for instance, the element peclet number. The difficulty is not peculiar to finite elements method as complexities are observed in most spatial discretization techniques [21]. Difficulties are also encountered when Characteristic Galerkin scheme is applied to obtain solutions for the momentum equation. However, the application and the incorporation of Characteristic Based Split (CBS) scheme into the finite element software/codes provides a permanent solution to this problem. The scheme satisfies the well-known Babuska-Brezzi condition [19-21]. To the best of the authors' knowledge, the previous studies on the numerical simulations did not consider the pressure and temperature distributions, as well the velocity in the drying chamber. Therefore, in this work, a

finite element method was used to simulate the heat transfer behavior in a photovoltaic-powered forced convection solar dryer. For performance optimization in the solar dryer analysis, the effects of the following factors such as blower speeds, the chamber ratio of the solar dryer, on the pressure and temperature distributions, and the velocity in the drying chamber were investigated.

2. The Equipment

The photovoltaic solar dryer is made up of the blower, the collector box, the dry chamber, and the photovoltaic module as assembled and shown in Figure 1. The materials used for the work include; wood, metal sheet, wire mesh, Perspex, and rock wool (used for insulation at the connections to prevent loss of energy). The collector is made up of the absorber plate for collection of solar energy, collector box made of frame and box, and the transparent glazing cover made of Perspex. The wooden collector box provides channel for the airflow into the drying chamber, while the heated air increases its capacity to sustain the water vapour. The dimensions of the drying chamber are 120 x 75 x 15 cm^3. The thermal conductivity of the aluminum sheet is 204 W/m-K and it is used for the absorber. It is painted in black color to enhance its absorptivity and emissivity of the radiant energy. The use of Perspex instead of glass was due to its relative elasticity, easy transportability and handling and its malleability and crack resistance under great amount of sunlight. From inclination theory, an angle of 16^0 is chosen and used for its inclination. There is an opening made of transparent glass at the backside of the drying chamber which allows the chamber to be viewed from the backside. The chamber has two mesh trays made of wood where the farm produce are kept. The photovoltaic-blower assembly is made up of the 11W photovoltaic panel, 12V DC blower for the air flow and moisturized air evacuation from the drying chamber in order to prevent moisture stagnation in the chamber.

3. The Solar Chamber

The Solar chamber is an enclosure where the product is dried and protected against insect, pest, rodent, duct and rain from damaging agricultural product. The inlet air increases in temperature by solar collector and channel through the drying chamber for drying the products. Blower/Fan is used to force heated air along the passage of drying chamber so as to dehydrate the product.

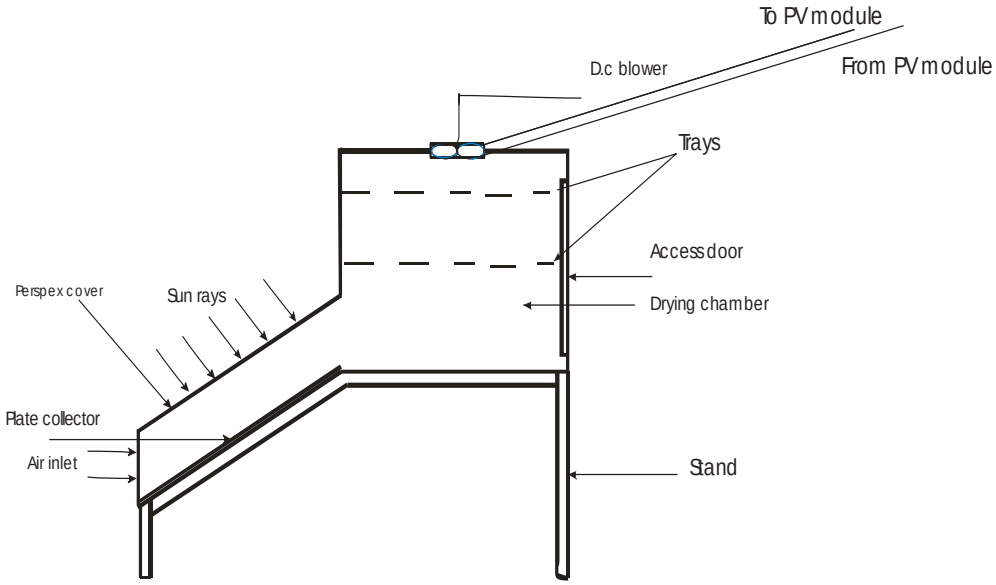

Fig. 1 Photo-voltaic forced convection solar dryer

4. Model Formulation: Solar Dryer

The Finite Element Simulation of the heat transfer process in solar dryer involves setting up heat transfer models. The model equation formulation includes the conservation equation.

Conservation Equations Formulation of Solar Dryer Chamber

The finite element method was applied to obtain solution for the resulting conservation equations

Continuity Equation

$$\frac{\partial u}{\partial x} + \frac{\partial v}{\partial y} = 0 \tag{1}$$

x-momentum equation

$$\frac{\partial u}{\partial t} + u\frac{\partial u}{\partial x} + v\frac{\partial u}{\partial y} = -\frac{1}{\rho}\frac{\partial p}{\partial x} + \nu\left[\frac{\partial^2 u}{\partial x^2} + \frac{\partial^2 u}{\partial y}\right] \tag{2}$$

y-momentum equation

$$\frac{\partial v}{\partial t} + u\frac{\partial v}{\partial x} + v\frac{\partial v}{\partial y} = -\frac{1}{\rho}\frac{\partial p}{\partial y} + v\left[\frac{\partial^2 v}{\partial x^2} + \frac{\partial^2 v}{\partial y^2}\right] \quad (3)$$

Energy Equation

$$\frac{\partial T}{\partial t} + u\frac{\partial T}{\partial x} + v\frac{\partial T}{\partial y} = \alpha\left[\frac{\partial^2 T}{\partial x^2} + \frac{\partial^2 T}{\partial y^2}\right] \quad (4)$$

The initial condition is given as

$$t = 0, \quad u = 0, \quad v = 0, \quad T = T_\infty, \quad p = p_\infty \quad for\ 0 < x < L, \quad 0 < y < H$$

The boundary conditions are given as :

$$t > 0, \quad y = 0, \quad u = v = 0, \quad \frac{\partial T}{\partial y} = 0, \quad \frac{\partial p}{\partial y} = 0 \quad 0 < x < L$$

$$t > 0, \quad y = H, \quad u = v = 0, \quad \frac{\partial T}{\partial y} = 0, \quad \frac{\partial p}{\partial y} = 0 \quad 0 < x < 0.4L$$

$$t > 0, \quad y = H, \quad u = 0, v = U_c, \quad T = T_c, \quad p = p_\infty \quad 0.4L < x < 0.6L$$

$$t > 0, \quad y = H \quad u = v = 0, \quad \frac{\partial T}{\partial y} = 0, \quad \frac{\partial p}{\partial x} = 0 \quad 0.6L < x < L$$

$$t > 0, \quad x = 0, \quad u = U_\infty, \quad v = 0, \quad T = T_h, \quad p = p_m \quad 0 < y < 0.3H$$

$$t > 0, \quad x = 0 \quad u = v = 0, \quad \frac{\partial T}{\partial x} = 0, \quad \frac{\partial p}{\partial x} = 0 \quad 0.3H < y < H$$

$$t > 0, \ x = L \quad u = v = 0, \ \frac{\partial T}{\partial x} = 0, \ \frac{\partial p}{\partial x} = 0 \quad 0 < y < H \quad (5a)$$

The non-dimensionalized form of the equation was obtained by applying the non-dimentional scales as follows.

$$X = \frac{x}{L}\ ,\ Y = \frac{y}{H},\ \ \tau = \frac{tu_\infty}{L},\ \ U = \frac{u}{U_\infty},\ \ V = \frac{v}{U_\infty},\ \ P = \frac{p}{\rho U^2{}_\infty},\ \theta = \frac{T-T_\infty}{T_w-T_\infty} \qquad (5b)$$

With the substitution of the non-dimentional parameters into the equations (1-4), we obtain:

Continuity equation

$$\frac{\partial U}{\partial X} + \frac{\partial V}{\partial Y} = 0 \qquad (6)$$

X-momentum equation

$$\frac{\partial V}{\partial \tau} + U\frac{\partial U}{\partial X} + V\frac{\partial U}{\partial Y} = -\frac{\partial P}{\partial Y} + \frac{1}{Re}\left(\frac{\partial^2 U}{\partial X^2} + \frac{\partial^2 U}{\partial Y^2}\right) \qquad (7)$$

Y-momentum equation

$$\frac{\partial V}{\partial \tau} + U\frac{\partial V}{\partial X} + V\frac{\partial V}{\partial Y} = -\frac{\partial P}{\partial Y} + \frac{1}{Re}\left(\frac{\partial^2 V}{\partial X^2} + \frac{\partial^2 V}{\partial Y^2}\right) \qquad (8)$$

Energy Equation

$$\frac{\partial \theta}{\partial \tau} + U\frac{\partial \theta}{\partial X} + V\frac{\partial \theta}{\partial Y} = \frac{1}{RePr}\left(\frac{\partial^2 \theta}{\partial X^2} + \frac{\partial^2 \theta}{\partial Y^2}\right) \qquad (9)$$

or

$$\frac{\partial \theta}{\partial \tau} + U\frac{\partial \theta}{\partial X} + V\frac{\partial \theta}{\partial Y} = \frac{1}{Pe}\left(\frac{\partial^2 \theta}{\partial X^2} + \frac{\partial^2 \theta}{\partial Y^2}\right) \qquad (10)$$

The initial condition is given as

$$\tau = 0, \quad U = 0, \quad U = 0, \quad \theta = 0, \ P = \frac{p_\infty}{\rho U_\infty^2} \qquad 0 < X < L, \qquad 0 < Y < L$$

The boundary conditions in the non-dimentional scales are:

$$\tau > 0, \ \ Y = 0, \quad U = V = 0, \quad \frac{\partial \theta}{\partial Y} = 0, \quad \frac{\partial P}{\partial Y} = 0 \qquad 0 < X < 1$$

$$\tau > 0, \quad Y = 1, \quad U = V = 0, \quad \frac{\partial \theta}{\partial Y} = 0, \quad \frac{\partial P}{\partial Y} = 0 \qquad 0 < X < 0.4$$

$$\tau > 0, \quad Y = 1, \quad U = \frac{U_c}{U_\infty}, \quad V = 0, \quad \theta = 0,$$
$$P = p_\infty / \rho U^2 \qquad 0.4 < X < 0.6$$

$$\tau > 0, \quad Y = 1 \quad U = V = 0, \quad \frac{\partial \theta}{\partial Y} = 0,$$
$$\frac{\partial P}{\partial X} = 0 \qquad 0.6 < Y < 1$$

$$\tau > 0, \quad X = 0, \quad U = 1, \quad V = 0, \quad T = 1,$$
$$P = p_m / \rho U^2 \qquad 0 < Y < 0.3$$

$$\tau > 0, \quad X = 0 \quad U = V = 0, \quad \frac{\partial \theta}{\partial X} = 0,$$
$$\frac{\partial P}{\partial X} = 0 \qquad 0.3 < Y < 1$$

$$\tau > 0, \quad X = L \quad U = V = 0, \quad \frac{\partial \theta}{\partial X} = 0, \quad \frac{\partial P}{\partial X} = 0 \qquad 0 < Y < 1$$

(11)

Finite Element Analysis for the Characteristics-Based Split (CBS) Conservation Equations

Continuity Equation results into

$$\frac{U_{i+1,j}^n - U_{i,j}^n}{\Delta X} + \frac{V_{i+1,j}^n - V_{i,j}^n}{\Delta Y} = 0 \quad \text{or} \quad \frac{\partial U_{ij}^n}{\partial X} + \frac{\partial V_{ij}^n}{\partial Y} = 0 \tag{12}$$

x momentum equation becomes a semi-discrete form as follows:

$$\frac{U_{ij}^{n+1} - U_{ij}^n}{\Delta \tau} = U_{ij}^n \frac{\partial U_{ij}^n}{\partial X} - V_{ij}^n \frac{\partial U_{ij}^n}{\partial Y} + \frac{1}{Re}\left(\frac{\partial^2 U_{ij}}{\partial X^2} + \frac{\partial^2 U_{ij}}{\partial Y^2}\right)^n - \frac{\partial P_{ij}}{\partial X} + U_{ij} \frac{\Delta \tau}{2} \frac{\partial}{\partial X}\left[U_{ij}^n \frac{\partial U_{ij}^n}{\partial X} + V_{ij}^n \frac{\partial U_{ij}^n}{\partial Y} + \frac{\partial P_{ij}^n}{\partial X}\right] + V_{ij} \frac{\Delta \tau}{2} \frac{\partial}{\partial Y}\left[U_{ij}^n \frac{\partial U_{ij}^n}{\partial X} + V_{ij}^n \frac{\partial U_{ij}^n}{\partial Y} + \frac{\partial P_{ij}^n}{\partial X}\right] \tag{13a}$$

y momentum equation becomes a semi-discrete form as follows:

$$\frac{V_{ij}^{n+1}-V_{ij}^{n}}{\Delta\tau}=U_{ij}^{n}\frac{\partial V_{ij}^{n}}{\partial X}-V_{ij}^{n}\frac{\partial V_{ij}^{n}}{\partial Y}+\frac{1}{Re}\left(\frac{\partial^2 V_{ij}}{\partial X^2}+\frac{\partial^2 V_{ij}}{\partial Y^2}\right)^{n}-\frac{\partial P_{ij}}{\partial X}+{U_{ij}}^{n}\frac{\Delta\tau}{2}\frac{\partial}{\partial X}\left[U_{ij}^{n}\frac{\partial U_{ij}^{n}}{\partial X}+V_{ij}^{n}\frac{\partial U_{ij}^{n}}{\partial Y}+\frac{\partial P_{ij}^{n}}{\partial X}\right]+{V_{ij}}^{n}\frac{\Delta\tau}{2}\frac{\partial}{\partial Y}\left[U_{ij}^{n}\frac{\partial V_{ij}^{n}}{\partial X}+V_{ij}^{n}\frac{\partial V_{ij}^{n}}{\partial Y}+\frac{\partial P_{ij}^{n}}{\partial X}\right]+\frac{Gr}{Re^2}\theta_{ij}^{n} \quad (13b)$$

When the pressure term is removed from equations 13a and 13b, equation 14-15 are obtained

$$\frac{U_{ij}-U_{ij}^{n}}{\Delta\tau}=U_{ij}^{n}\frac{\partial U_{ij}^{n}}{\partial X}-V_{ij}^{n}\frac{\partial U_{ij}^{n}}{\partial Y}+\frac{1}{Re}\left(\frac{\partial^2 U_{ij}}{\partial X^2}+\frac{\partial^2 U_{ij}}{\partial Y^2}\right)^{n}+{U_{ij}}^{n}\frac{\Delta\tau}{2}\frac{\partial}{\partial X}\left(U_{ij}^{n}\frac{\partial U_{ij}^{n}}{\partial X}+V_{ij}^{n}\frac{\partial U_{ij}^{n}}{\partial Y}\right)+V_{ij}^{n}\frac{\Delta\tau}{2}\frac{\partial}{\partial Y}\left(U_{ij}^{n}\frac{\partial U_{ij}^{n}}{\partial X}+V_{ij}^{n}\frac{\partial U_{ij}^{n}}{\partial Y}\right) \quad (14)$$

$$\frac{V_{ij}-V_{ij}^{n}}{\Delta\tau}=U_{ij}^{n}\frac{\partial V_{ij}^{n}}{\partial X}-V_{ij}^{n}\frac{\partial V_{ij}^{n}}{\partial Y}+\frac{1}{Re}\left(\frac{\partial^2 V_{ij}}{\partial X^2}+\frac{\partial^2 V_{ij}}{\partial Y^2}\right)^{n}+U_{ij}^{n}\frac{\Delta\tau}{2}\frac{\partial}{\partial X}\left(U_{ij}^{n}\frac{\partial U_{ij}^{n}}{\partial X}+V_{ij}^{n}\frac{\partial U_{ij}^{n}}{\partial Y}\right)+V_{ij}^{n}\frac{\Delta\tau}{2}\frac{\partial}{\partial Y}\left(U_{ij}^{n}\frac{\partial V_{ij}^{n}}{\partial X}+V_{ij}^{n}\frac{\partial V_{ij}^{n}}{\partial Y}\right)+\frac{Gr}{Re^2}\theta_{ij}^{n} \quad (15)$$

When equation 14 and 15 are subtracted from equations 13a and 13b separately, the real velocity field equations are obtained. (momentum or velocity correction equations) as:

$$\frac{U_{ij}^{n+1}-\widetilde{U}_{ij}}{\Delta\tau}=-\frac{\partial P^{n}}{\partial X}+U\frac{\Delta\tau}{2}\frac{\partial}{\partial X}\left(\frac{\partial P}{\partial X}\right)^{n}+V\frac{\Delta\tau}{2}\frac{\partial}{\partial X}\left(\frac{\partial P}{\partial X}\right)^{n} \quad (16)$$

$$\frac{V_{ij}^{n+1}-\widetilde{V}_{ij}}{\Delta\tau}=-\frac{\partial P^{n}}{\partial Y}+U\frac{\Delta\tau}{2}\frac{\partial}{\partial X}\left(\frac{\partial P}{\partial X}\right)^{n}+V\frac{\Delta\tau}{2}\frac{\partial}{\partial Y}\left(\frac{\partial P}{\partial Y}\right)^{n} \quad (17)$$

When equation 17 is differentiated further with respect to *x* and *y*, while combining the obtained equations while neglecting the observed third-order terms in the equation yields;

$$\frac{\partial U_{ij}^{n+1}}{\partial \mathrm{X}}+\frac{\partial V_{ij}^{n+1}}{\partial \mathrm{Y}}-\frac{\partial \tilde{U}_{ij}}{\partial X}-\frac{\partial \tilde{V}_{ij}}{\partial Y}=-\Delta\tau\left(\frac{\partial^2 P_{ij}}{\partial X^2}+\frac{\partial^2 P_{ij}}{\partial Y^2}\right)^n \tag{18}$$

Which gives the pressure caculation

$$\left(\frac{\partial^2 P_{ij}}{\partial X^2}+\frac{\partial^2 P_{ij}}{\partial Y^2}\right)^n=\frac{1}{\Delta\tau}\left(\frac{\partial \tilde{U}_{ij}}{\partial X}^n+\frac{\partial \tilde{V}_{ij}}{\partial Y}^n\right) \tag{19}$$

Since (continuity equation);

$$\frac{\partial U_{ij}^{n+1}}{\partial \mathrm{X}}+\frac{\partial V_{ij}^{n+1}}{\partial \mathrm{Y}}=0 \tag{20}$$

Determining the Temperature

When the characteristic Galerkin procedure is applied to the temperature equation (11), the resulting equations become:

$$\frac{\theta_{ij}^{n+1}-\theta_{ij}^{n}}{\Delta t}=U_{ij}^{n}\frac{\partial \theta^{n}}{\partial X}-V_{ij}^{n}\frac{\partial \theta_{ij}^{n}}{\partial Y}+\frac{1}{RePr}\left(\frac{\partial^2 \theta_{ij}}{\partial X^2}+\frac{\partial^2 \theta_{ij}}{\partial Y^2}\right)^n+U\frac{\Delta\tau}{2}\frac{\partial}{\partial X}\left(U\frac{\partial \theta}{\partial X}+V\frac{\partial \theta}{\partial Y}\right)+V\frac{\Delta\tau}{2}\frac{\partial}{\partial Y}\left(U\frac{\partial \theta}{\partial X}+V\frac{\partial \theta}{\partial Y}\right)^n \tag{21}$$

The intermediate *x*-momentum equation is summarizes as follows:

$$\frac{\tilde{U}_{ij}-\tilde{U}_{ij}^{n}}{\Delta t}=U\frac{\partial U_{ij}^{n}}{\partial X}-V\frac{\partial U_{ij}^{n}}{\partial X}+\frac{1}{Re}\left(\frac{\partial^2 U_{ij}}{\partial X^2}+\frac{\partial^2 U_{ij}}{\partial Y^2}\right)^n+U_{ij}^{n}\frac{\Delta\tau}{2}\frac{\partial}{\partial X}\left(U_{ij}^{n}\frac{\partial V_{ij}}{\partial X}+V\frac{\partial V_{ij}}{\partial Y}\right)^n+V_{ij}^{n}\frac{\Delta\tau}{2}\frac{\partial}{\partial Y}\left(U_{ij}^{n}\frac{\partial U_{ij}}{\partial X}+V\frac{\partial U_{ij}}{\partial Y}\right) \tag{22}$$

And the intermediate *y*-momentum equation is:

$$\frac{\tilde{V}_{ij}-\tilde{V}_{ij}^{n}}{\Delta t}=U_{ij}\frac{\partial V_{ij}^{n}}{\partial X}-V\frac{\partial V_{ij}^{n}}{\partial Y}+\frac{1}{Re}\left(\frac{\partial^2 V_{ij}}{\partial X^2}+\frac{\partial^2 V_{ij}}{\partial Y^2}\right)^n+U_{ij}^{n}\frac{\Delta\tau}{2}\frac{\partial}{\partial X}\left(U_{ij}^{n}\frac{\partial V_{ij}}{\partial X}+V\frac{\partial V_{ij}}{\partial Y}\right)^n+V_{ij}^{n}\frac{\Delta\tau}{2}\frac{\partial}{\partial Y}\left(U\frac{\partial U_{ij}}{\partial X}+V\frac{\partial U_{ij}}{\partial Y}\right) \tag{23}$$

Pressure Calculation

$$\left(\frac{\partial^2 P_{ij}}{\partial X^2}+\frac{\partial^2 P_{ij}}{\partial Y^2}\right)^n=\frac{1}{\Delta\tau}\left(\frac{\partial \widetilde{U}_1}{\partial X}+\frac{\partial \widetilde{V}}{\partial Y}\right) \quad (24)$$

Temperature equation

$$\frac{\theta_{ij}^{n+1}-\theta_{ij}^{n}}{\Delta t}=U_{ij}^{n}\frac{\partial \theta^n}{\partial X}-V_{ij}^{n}\frac{\partial \theta_{ij}^{n}}{\partial Y}+\frac{1}{RePr}\left(\frac{\partial^2 \theta_{ij}}{\partial X^2}+\frac{\partial^2 \theta_{ij}}{\partial Y^2}\right)^n+U\frac{\Delta\tau}{2}\frac{\partial}{\partial X}\left(U\frac{\partial \theta}{\partial X}+V\frac{\partial \theta}{\partial Y}\right)+V\frac{\Delta\tau}{2}\frac{\partial}{\partial Y}\left(U\frac{\partial \theta}{\partial X}+V\frac{\partial \theta}{\partial Y}\right)^n \quad (25)$$

Spatial Discretization

The standard Galerkin approximation method is applied to obtain solutions for equations 20-25, the linear interpolation functions are applied for the used variables, and then the linear triangular element spatial discretization is written as follows:

$$U=N_iU_i+N_jU_j+N_kU_k=[N][U] \quad (26)$$

$$V=N_iV_i+N_jV_j+N_kV_k=[N][V] \quad (27)$$

$$P=N_iP_i+N_jP_j+N_kP_k=[N][P] \quad (28)$$

$$\theta=N_i\theta_i+N_j\theta_j+N_k\theta_k=[N][\theta] \quad (29)$$

The obtained Mass Element Matrix from the Characteristics-Based Split scheme following the spatial discretization is

$$[M_e]=\frac{A}{12}\begin{bmatrix}2&1&1\\1&2&1\\1&1&2\end{bmatrix} \quad (30)$$

And the Element Convection Matrix

$$[C_e] = \frac{1}{24}\begin{bmatrix} (wsw+u_i)b_i & (wsw+u_i)b_j & (wsw+u_i)b_k \\ (wsw+u_j)b_i & (wsw+u_j)b_j & (wsw+u_j)b_k \\ (wsw+u_k)b_i & (wsw+u_k)b_j & (wsw+u_k)b_k \end{bmatrix} + \frac{1}{24}\begin{bmatrix} (wrw+u_i)c_i & (wrw+u_i)c_j & (wrw+u_i)c_k \\ (wrw+u_j)c_i & (wrw+u_j)c_j & (wrw+u_j)c_k \\ (wrw+u_k)c_i & (wrw+u_k)c_j & (wrw+u_k)c_k \end{bmatrix} \quad (31)$$

Where

$$wsw = u_i + u_j + u_k$$

$$wrw = v_i + v_j + v_k$$

$$[K_e] = \frac{Re}{4A}\begin{bmatrix} b_i^2 & b_j b_i & b_k b_i \\ b_i b_j & b_j^2 & b_k b_j \\ b_i b_k & b_j b_k & b_k^2 \end{bmatrix} + \frac{Re}{4A}\begin{bmatrix} c_i^2 & c_j c_i & c_k c_i \\ c_i c_j & c_j^2 & c_k c_j \\ c_i c_k & c_j c_k & c_k^2 \end{bmatrix} \quad (32)$$

For the momentum diffussion, we have;

$$[K_{te}] = \frac{P_r}{4A}\begin{bmatrix} b_i^2 & b_j b_i & b_k b_i \\ b_i b_j & b_j^2 & b_k b_j \\ b_i b_k & b_j b_k & b_k^2 \end{bmatrix} + \frac{P_r}{4A}\begin{bmatrix} c_i^2 & c_j c_i & c_k c_i \\ c_i c_j & c_j^2 & c_k c_j \\ c_i c_k & c_j c_k & c_k^2 \end{bmatrix} \quad (33)$$

The Heat diffusion and Stabilization Matrices are also obtained as follows

$$[K_{se}] = \frac{U_{av}}{12}\begin{bmatrix} b_i^2 & b_j b_i & b_k b_i \\ b_i b_j & b_j^2 & b_k b_j \\ b_i b_k & b_j b_k & b_k^2 \end{bmatrix} + \frac{U_{av}}{12}\begin{bmatrix} b_i c_i & b_i c_j & b_i c_k \\ b_j c_i & b_j c_j & b_j c_k \\ b_k c_i & b_k c_j & b_k c_k \end{bmatrix} + \frac{V_{av}}{12A}\begin{bmatrix} c_i b_i & c_i b_j & c_i b_k \\ c_j b_i & c_j b_j & c_j b_k \\ c_k b_i & c_k b_j & c_k b_k \end{bmatrix} + \frac{V_{av}}{12A}\begin{bmatrix} c_i^2 & c_i c_j & c_i c_k \\ c_j c_i & c_j^2 & c_j c_k \\ c_k c_i & c_k c_j & c_k^2 \end{bmatrix} \quad (34)$$

Where $U_{av}$and V_{av} are the mean values of U and V for the elements. In order to complete the solution process, the spatial discretization of the Characteristics-Based Split scheme involves more forcing vectors and matrices. The discretized results yields the matrix forthe second-order terms for the pressure parameter is:

$$K = \frac{1}{4A}\begin{bmatrix} b_i^2 & b_j b_i & b_k b_i \\ b_i b_j & b_j^2 & b_k b_j \\ b_i b_k & b_j b_k & b_k^2 \end{bmatrix} + \frac{1}{4A}\begin{bmatrix} c_i^2 & c_i c_j & c_i c_k \\ c_j c_i & c_j^2 & c_j c_k \\ c_k c_i & c_k c_j & c_k^2 \end{bmatrix} \quad (35)$$

The first gradient matrix as obtained for the x-direction is:

$$[G_u] = \frac{1}{6}\begin{bmatrix} b_i & b_j & b_k \\ b_i & b_j & b_k \\ b_i & b_j & b_k \end{bmatrix} \quad (36)$$

While the second-gradient matrix as obtained for the y-direction is

$$[G_v] = \frac{1}{6}\begin{bmatrix} c_i & c_j & c_k \\ c_i & c_j & c_k \\ c_i & c_j & c_k \end{bmatrix} \quad (37)$$

The obtained forcing vectors of the x-component for momentum equation is:

$$[f_1] = \frac{\Gamma}{4A} Re \begin{bmatrix} b_i u_i & b_j u_j & b_k u_k \\ b_i u_i & b_j u_j & b_k u_k \\ 0 & 0 & 0 \end{bmatrix}^n n_u + \frac{\Gamma}{4A} Re \begin{bmatrix} c_i u_i & c_j u_j & c_k u_k \\ c_i u_i & c_j u_j & c b_k u_k \\ 0 & 0 & 0 \end{bmatrix}^n n_v \quad (38)$$

Where $i\ j$ is the boundary edge of an element.

The obtained forcing vector of the y- component momentum equation is:

$$[f_2] = \frac{\Gamma}{4A} Re \begin{bmatrix} b_i v_i & b_j v_j & b_k v_k \\ b_i v_i & b_j v_j & b_k v_k \\ 0 & 0 & 0 \end{bmatrix}^n n_u + \frac{\Gamma}{4A} Re \begin{bmatrix} c_i v_i & c_j v_j & c_k v_k \\ c_i v_i & c_j v_j & c_k v_k \\ 0 & 0 & 0 \end{bmatrix}^n n_v \quad (39)$$

The obtained forcing vector using the discretization of the second-order of pressure terms in the calculation of pressure is as follows:

$$[f_3] = \frac{\Gamma}{4A} \begin{bmatrix} b_i P_i & b_j P_j & b_k P_k \\ b_i P_i & b_j P_j & b_k P_k \\ 0 & 0 & 0 \end{bmatrix}^n n_u + \frac{\Gamma}{4A} \begin{bmatrix} c_i P_i & c_j P_j & c_k P_k \\ c_i P_i & c_j P_j & c_k P_k \\ 0 & 0 & 0 \end{bmatrix}^n n_v \quad (40)$$

Finally, the obtained forcing vector term using the discretization of the pressure term in the second-order is:

$$[f_4] = \frac{\Gamma}{4A} Pr \begin{bmatrix} b_i \theta_i & b_j \theta_j & b_k \theta_k \\ b_i \theta_i & b_j \theta_j & b_k \theta_k \\ 0 & 0 & 0 \end{bmatrix}^n n_u + \frac{\Gamma}{4A} P_r \begin{bmatrix} c_i \theta_i & c_j \theta_j & c_k \theta_k \\ c_i \theta_i & c_j \theta_j & c_k \theta_k \\ 0 & 0 & 0 \end{bmatrix}^n n_v \quad (41)$$

The Matrix form of the four steps for the characteristic based split scheme is as follows.

Step 1: Calculations of the Intermediate Velocity in the x-Component

$$\left[M\frac{\Delta[\widetilde{U}]}{\Delta t}\right]=[f_1]-[C][U]^n-[K_m][U]^n-[K_b][U]^n \quad (42)$$

Calculations of the Intermediate Velocity in the y-Component

$$\left[M\frac{\Delta[\widetilde{U}]}{\Delta t}\right]=[f_2]-[C][V]^n-[K_m][V]^n-[K_s][V]^n \quad (43)$$

Step 2: Calculation for Pressure

$$[K][P]^n=[f_3]-\frac{1}{\Delta t}[G_u]\left[\widetilde{U}\right]+[G_u]\left[\widetilde{V}\right] \quad (44)$$

Step 3: Correction of Velocity term

$$[M][U]^{n+1}=[M]\left[\widetilde{U}\right]-\Delta\tau[G_v][P]^n \quad (45a)$$

$$[M][V]^{[n+1}=[M]\left[\widetilde{V}\right]-\Delta\tau[G_v][P]^n \quad (45b)$$

Step 4: Computation of Temperature term

$$\left[M\frac{\Delta[\theta]}{\Delta t}\right]=[f_4]-[C][\theta]^n-\left[K_f\right][\theta]^n-[K_s][\theta]^n \quad (46)$$

5. Results and Discussion

The figures in the results shown above display the variation and the distributions in colours and contours for the different blower speeds and aspect ratios. These results showed the air dynamics drying chamber for 2000 sec of highest insolation.

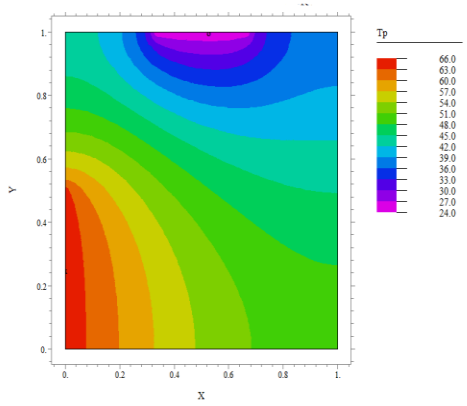

Fig. 2 Temperature Distribution in the drying chamber at an Aspect ratio (L/H) of 1 and Blower speed 0.2m/s

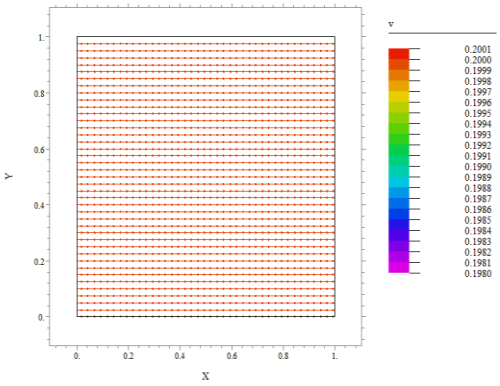

Fig. 3 Velocity Distribution in the drying chamber at an Aspect ratio (L/H) of 1 and Blower speed 0.2m/s

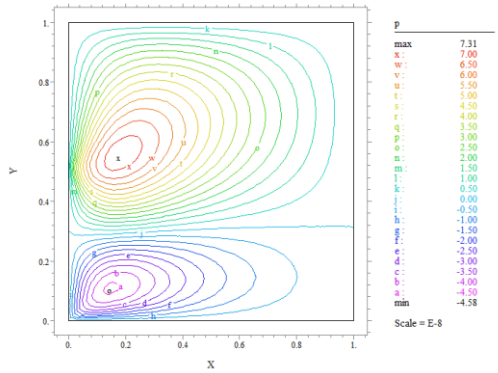

Fig. 4 Pressure Distribution in the drying chamber at an Aspect ratio (L/H) of 1 and Blower speed 0.2m/s

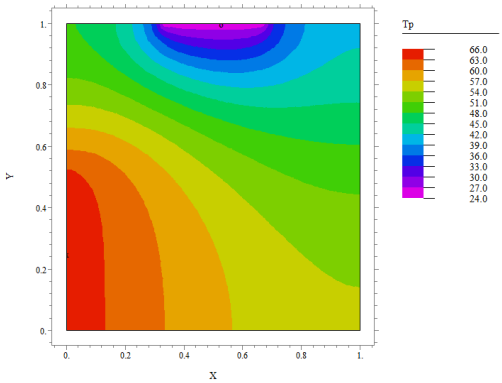

Fig. 5 Temperature Distribution in the drying chamber at an Aspect ratio (L/H) of 1 and Blower speed 0.6m/s

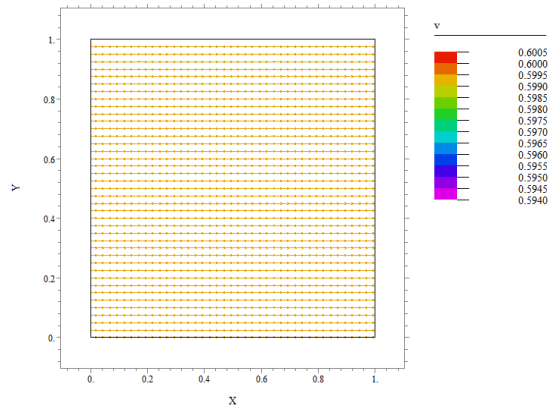

Fig. 6 Velocity Distribution in the drying chamber at an Aspect ratio (L/H) of 1 and Blower speed 0.6m/s

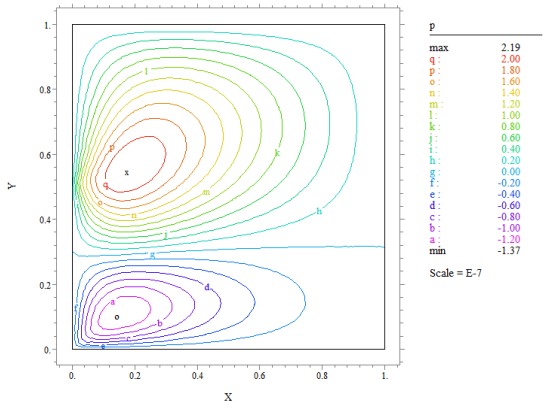

Fig. 7 Pressure Distribution in the drying chamber at an Aspect ratio (L/H) of 1 and Blower speed 0.6m/s

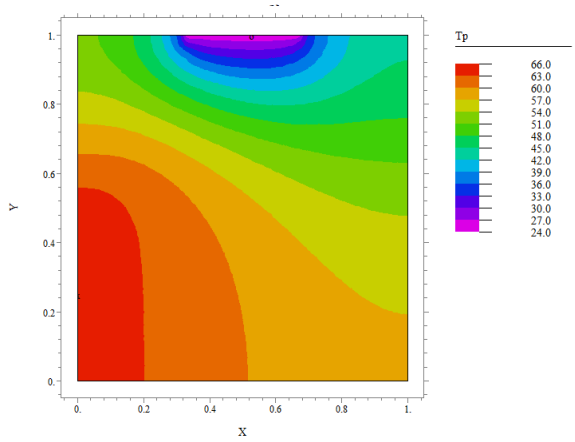

Fig. 8 Temperature Distribution in the drying chamber at an Aspect ratio (L/H) of 1 and Blower speed 1.0m/s

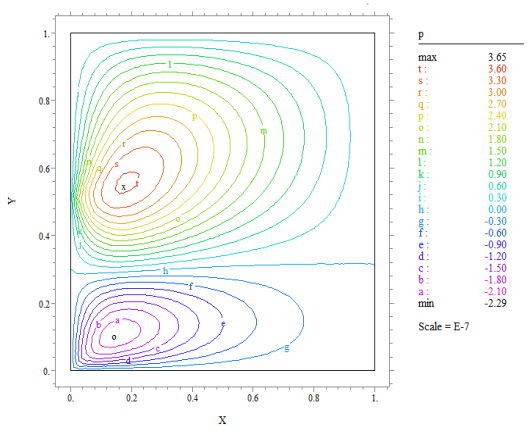

Fig. 9 Pressure Distribution in the drying chamber at an Aspect ratio (L/H) of 1 and Blower speed 1.0m/s

Fig. 2-9 show the temperature, pressure and velocity distributions of the drying chamber of an aspect ratio 1 for the blower speeds of 0.2 m/s, 0.4 m/s, 0.6 m/s and 1 m/s. From these results, it could be seen that the space achieved by the maximum temperature of 65 ^{o}C in the drying chamber tends to increase in the chamber as the speed of the blower increases. However, as the blower speed increases, pressure reduces in the drying chamber and the velocity of the hot air in the drying chamber increases.

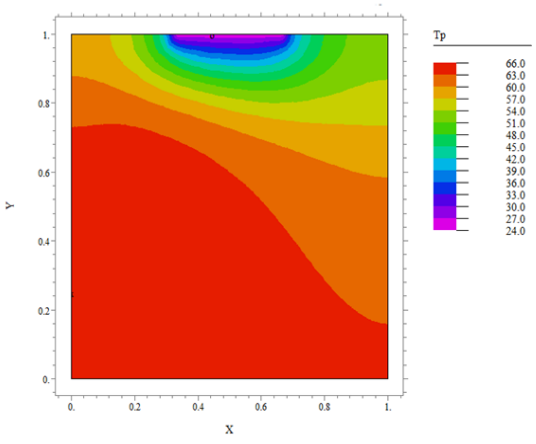

Fig. 10 Temperature Distribution in the drying chamber at an Aspect ratio (L/H) of 1 and Blower speed 3.0m/s

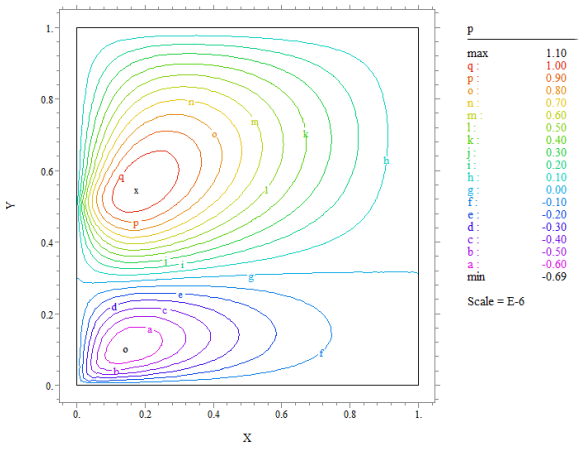

Fig. 11. Pressure Distribution in the drying chamber at an Aspect ratio (L/H) of 1 and Blower speed 3.0m/s

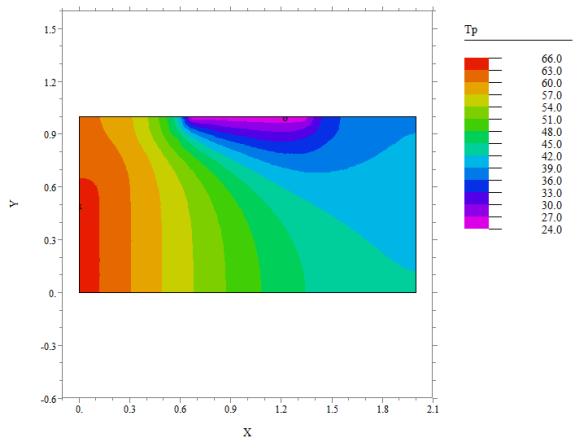

Fig. 12 Temperature Distribution in the drying chamber at an Aspect ratio (L/H) of 2 and Blower speed 3.0m/s

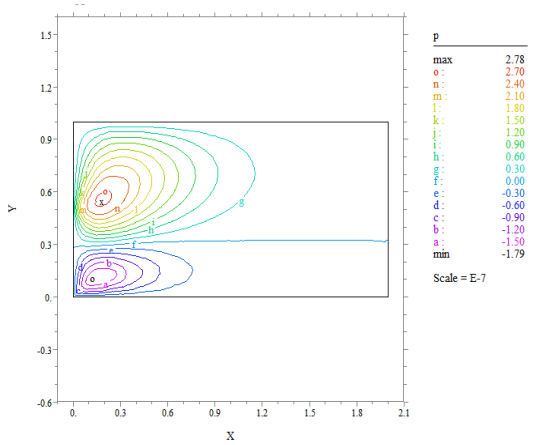

Fig. 13 Pressure Distribution in the drying chamber at an Aspect ratio (L/H) of 2 and Blower speed 3.0m/s

The results of the temperature and pressure distributions in the drying chamber of an aspect ratio 1 for the blower speeds of 3 m/s are shown in Figures 10 and 11, while Figures12 and 13 show the temperature and pressure distribution in the drying chamber of an aspect ratio 2 for the blower speed of 3m/s. As depicted by the figures, the space achieved by the maximum temperature when the aspect ratio is 2 was found to be reduced as compared to the aspect ratio of 1 and this shows that performance of the drying chamber with the same blower speed of 3 m/s drops at an increase aspect ratio.

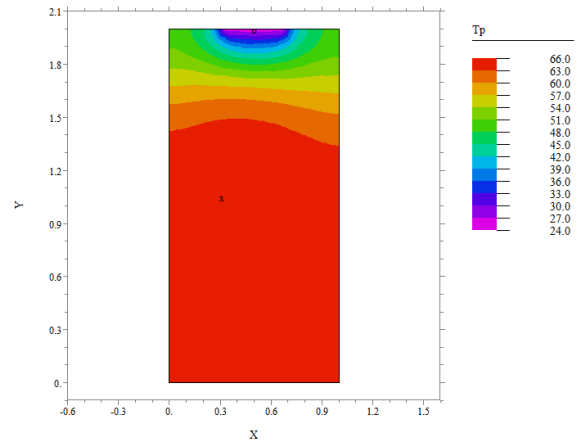

Fig. 14 Temperature Distribution in the drying chamber at an Aspect ratio (L/H) of 0.5 and Blower speed 3.0m/s 3.0m/s

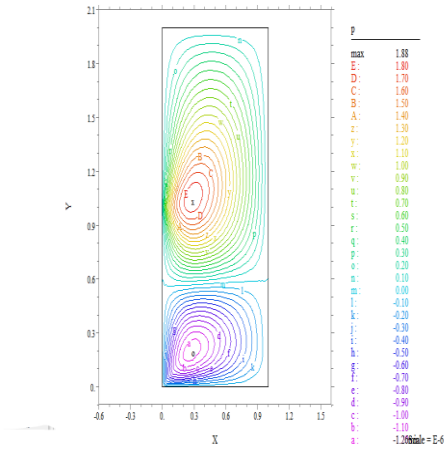

Fig.15 Pressure Distribution in the drying chamber at an Aspect ratio (L/H) of 0.5 and Blower speed

Fig.14 and 15 show the temperature and pressure distribution in the drying chamber of an aspect ratio 0.5 and blower speed of 3ms. From the figures, the space achieved by the maximum temperature increased significantly and the chamber seem to quickly attain a uniform maximum temperature of 65^{o}C over a wide range of space in the drying chamber and this show that performance of the drying chamber with the same blower speed of 3 m/s increases at a reduced aspect ratio. It could therefore be deduced from the results that the performance of the drying chamber increases as its aspect ratio decreases and the blower speed increases. An aspect ratio of 0.5 is recommended as an optimum value for the drying chamber as predicted in this work.

6. Conclusion

In this work, the finite element method has been applied to analyze the heat transfer and temperature behaviour in a forced-convective solar dryer powered by photovoltaic system. The effects of the following factors such as blower speeds, the chamber ratio of the solar dryer, on the pressure and temperature distributions as well as the velocity in the drying chamber were investigated. From the simulated results, the performance of the drying chamber increases as its aspect ratio decreases and the blower speed increases. Based on the findings in this work, It is therefore recommended that an aspect ratio of 0.5 could be used as an optimum value for the drying chamber. The results of this work could be used in the design of an optimised Photovoltaic-ventilated forced convection solar dryer.

Nomenclature

Pr Prandtl number

Re Reynold Number

Pe Peclet number

t time, s

T temperature, ^{o}C

T_w wall temperature, ^{o}C

T_∞ atmospheric temperature, ^{o}C

U dimensionless velocity along x-axis

u_∞ free stream velocity, m/s

V dimensionless velocity along x-axis

x length of the oven, m

X dimensionless length of the oven

y breadth of the oven

Y dimensionless breadth of the oven

Symbol

α thermal diffusivity, m^2/s

θ dimensionless temperature

τ dimensionless time

ρ density, kg/m^3

μ coefficient of dynamic viscosity, kg/ms

References

[1] T. A. Reddy, D. Pushparaj and C. L. Gupta C. L. A Design Procedure for Convective Solar Dryers' *Cong Solaire International*, *Nice*, 1979.

[2] J. Mumba. Development of a Photovoltaic Powered Forced Circulation Grain Dryer Used in the Tropics", *Renewable Energy*, 6(7)(1995), 885-862.

[3] P. H. Oosthuizen. The Design of Indirect Solar Rice Dryers, *Journal of Engineering for International Development*, 2(1)(1995), 20-27.
[4] G. Wisniewski and S. M. Pietruszko. Development of Solar Agricultural Dryers Combined with PV Modules and Solar Collectors", International Conference on Solar Energy at High Latitude N^0 7(1997), 215-221.
[5] A. O. Adelaja, B. Y. Ogunmola and P. O. Akolade. Development of a Photovoltaic powered Forced Convection Solar Dryer. Advanced Materials Research, 62-64(2009), 543-548.
[6] B. K. Bala and J. L. Woods, J. L. Simulation of the Indirect Natural Convection Solar Drying of Rough Rice, Solar Energy. 53(3)(1994), 259-266.
[7] B. K. Bala and J. L. Woods. Optimization of a Natural Convection Solar Drying System, *Energy*, 20(4)(1995), 285-294.
[8] K. Murugesan, K. N. Seetharamu, P. A. Narayana. A one dimensional analysis of convective drying of porous materials. Journal of Heat and Mass Transfer. 32(1)(1996):81-88.
[9] A. Gan and K. T. Choo K.T. Thermal performance ofa solar dryer-simulation case study, 2000, 134–152.
[10] I. N. Simate. Optimization of Mixed Mode and Indirect Mode Natural Convection Solar Dryers, *Renewable Energy*. 28(2003), 435-453.
[11] K. A. Ahmet, A. A. Orhan. Ibrahim Dincer Numerical modeling of heat and mass transfer during forced convection drying of rectangular moist objects International Journal of Heat and Mass Transfer. 49(2006), 3094–3103
[12] M. Aversa, S. Curcio, V. Calabro, G. Dorio, G. An analysis of the transport phenomena occurring during food drying process. Journal of Food Engineering, 78(3)(2007), 922-932.
[13] B. O. Bolaji and A. P. Olalusi, A. P. 2008: "Performance Evaluation of a Mixed-Mode Solar Dryer", *AU. J. T.*, 11(4)(2008), 225-231.
[14] B. K. Bala, M. D. Hossain and M. R. A. Mondol. Photovoltaic Based Forced Convection Solar Tunnel Dryer for Pineapple, Journal of Agricultural Engineering, 32(4(1997), 23-31.
[15] S. Janjai, T. Keawprasert, C. Chaicheet, P. Intawee, B. K. Bala and W. Muhlbaner. Simulation Model of a PV-Ventilated System for a Solar Dryer", *Technical Digest of the International PV SEC-14*, Bangkok, Thailand, 2004, 861-862.
[16] M. H. Ruslan, M. Othman, B. Yatim, K. Sopianand, Z. Ibarahim. Performance of V-groove forceconvective solar drying system, Asian-Oceania Conference, 2002.
[17] A. Kaya, C. Aydin, I. Dincer. Numerical modelling of heat and mass transfer during forced convection drying of rectangular moist objects. Journal of Heat and MassTransfer; Vol. 49(17)(2006), 3094-4103.
[18] A. Salah, M. H. Eltief, M., B. Y. Ruslan. Drying chamber performance of v-groove forced convective solar dryer desalination Vol. 209(2007), 151–155.
[19] B. Babuska. "The finite element method with Lagrangian multipliers," Numer. Math., 20(1973), 179-192.
[20] F. Brezzi, "On the existence, uniqueness and approximation of saddle-point problems arising from Lagrangian multipliers." RAIRO Ser. Rouge, 8(1994), 129-151.
[21] R. W. Lewis, P. Nithiarasu and K. N. Seetharamu. Fundamental of the Finite Element Method for Heat and Fluid Flow John Wiley and Sons, 2004.